scientific reports

Check for updates

OPEN

PNO1 enhances ovarian cancer cell growth, invasion, and stemness via activating the AKT/Wnt/β-catenin pathway

Lu Qin[1], Jiao Lu[1], Qiaohong Qian[2], Minjie Tang[2] & Min Liu[2]✉

PNO1, a key promoter of oncogenesis, is often characterized by its aberrant expression in both colorectal and esophageal cancers, markedly accelerating their progression. Nonetheless, the role of PNO1 in ovarian cancer and its underlying mechanisms remain unexplored comprehensively. In addition to the abnormal PNO1 expression in ovarian cancer tissues by The Cancer Genome Atlas (TCGA) database, the clinical data examinations indicated its strong association with lower survival rates among ovarian cancer patients. Considering the crucial role of the AKT signaling pathway, we hypothesized that PNO1 might drive the progression of ovarian cancer by modulating the AKT pathway. To validate this hypothesis, experiments were conducted to silence PNO1 in ovarian cancer cells. These findings demonstrated that PNO1 silencing markedly reduced the proliferation and invasion capabilities of ovarian cancer cell lines, triggering their apoptosis. Moreover, the PNO1 suppression significantly decreased the expression levels of p-AKT, GSK-3β, and active β-catenin proteins, further confirming the regulatory correlation between PNO1 and the AKT/Wnt/β-catenin pathway. The oncogenic effects mediated by the PNO1-activated Wnt/β-catenin pathway were counteracted by inhibitors of the AKT signaling pathway. Further, the subcutaneous xenograft tumor assays in vivo validated that PNO1 silencing decreased the tumorigenic potential of ovarian cancer cells. In summary, this study has elucidated that the upregulation of PNO1 modulated the tumorigenic role of the AKT/Wnt/β-catenin pathway in ovarian cancer, offering new insights into its oncogenic function.

Keywords PNO1, AKT, Ovarian cancer, GSK3-β, B-catenin

Cancer has emerged as one of the significant healthcare challenges in contemporary times, accounting for high incidence and progression rates. The complexity and diversity of tumor regulation accentuate the urgent need for the development of precise treatment strategies and explore a deeper understanding of the pathological mechanisms[1]. Among various kinds of gynecological cancers, ovarian cancer accounts for the high incidence rate, trailing only behind uterine and cervical cancers, leading to high mortality rates[2–6]. The high mortality rate of ovarian cancer is largely attributed to its location in the deep pelvic region, masking the early tumorigenesis symptoms and complicating its early diagnosis. Consequently, most ovarian cancers are diagnosed during the advanced stages[7,8]. Typically, the aggressive nature, high recurrence rate, and propensity for metastasis of ovarian cancer emphasize the critical need for further research into its mechanisms.

The eukaryotic cytoskeleton, comprising microtubules, microfilaments, and intermediate filaments, plays a vital role in maintaining the shape and function of cells. Cytokeratins, key components of the intermediate filament family, are predominantly found in epithelial cells. The *PNO1* gene, situated on chromosome 2p14, consists of eight exons encoding 210 amino acids. The *PNO1* gene is associated with small ribosomal subunit maturation and various cellular processes, including division, migration, differentiation, and apoptosis of cells[9–11]. Several studies reported abnormal PNO1 expression in several cancers, such as gastric osteosarcoma, lung adenocarcinoma, hepatocellular carcinoma, and esophageal cancer[9–11]. PNO1 expression was closely linked to tumor progression, often indicating a poor prognosis due to its role in promoting malignant proliferation.

[1]Department of Pathology, Jingjiang Traditional Chinese Medicine Hospital of Jiangsu Province, 29 Kangning Road, Jingjiang 214500, Jiangsu, China. [2]Department of Integrative Medicine, Obstetrics and Gynecology Hospital of Fudan University, No. 419, Fangxie Road, Shanghai 200011, Shanghai, China. ✉email: liumin7325@fckyy.org.cn

Although its specific role and mechanism in ovarian cancer remain to be elucidated, PNO1 emerges as a promising target for anticancer drug development.

AKT, a serine/threonine kinase, was first identified in an acutely transformed retrovirus-transduced oncogene from an AKR thymoma[12]. Several reports demonstrated the role of AKT as a pivotal signaling molecule in higher eukaryotes and a key kinase in human physiology and various diseases, particularly cancer[13,14]. AKT activation has been documented in numerous cancers, including breast, lung, pancreas, thyroid, and stomach cancers[15]. In an instance, AKT activation in ovarian cancer could lead to GSK-3β activation, triggering the Wnt/β-catenin signaling pathway[15–17]. Despite considerable investigation into AKT's upstream regulatory mechanisms, the role of PNO1 influencing the AKT/Wnt/β-catenin signaling pathway in ovarian cancer remains unexplored. Motivated by these findings, this study focused on elucidating the potential regulatory role of PNO1 in ovarian cancer. Despite extensive investigations into the upstream regulatory mechanisms governing AKT activity, the potential role of PNO1 in modulating the AKT/Wnt/β-catenin signaling axis within the context of ovarian cancer is also demonstrated.

Experimental section

Analysis of PNO1 expression and survival in ovarian cancer

The Gene Expression Profiling Interaction Analysis (GEPIA) tool (http://gepia.cancer-pku.cn/) was utilized to evaluate the PNO1 expression in human ovarian cancer. In addition, the PrognoScan database (http://dna00.bio.kyutech.ac.jp/PrognoScan/index.html) was employed to investigate the clinicopathological correlation of PNO1 expression with outcomes in ovarian cancer patients, including overall survival metrics.

Cell culture

Human ovarian cancer cell lines (CAOV3, SKOV3, OVCAR-3, and A2780) and the normal cell line IOSE80 were purchased from the American Type Culture Collection (ATCC, Manassas, USA). These cell lines were maintained in Roswell Park Memorial Institute (RPMI)-1640 medium (Gibco, Inc., Waltham, USA), supplemented with 10% fetal bovine serum (FBS) and 1% penicillin-streptomycin mixture (comprising 10,000 unit/mL penicillin and 10,000 μg/mL streptomycin, Gibco), within a CO_2 incubator set at 37 °C.

Collection of clinical samples

Fresh ovarian cancerous tissue samples were provided by Obstetrics & Gynecology Hospital of Fudan University, with all participants contributing to scientific research. The experimental protocols for this study were approved by the Ethics Committee and were conducted in accordance with the Declaration of Helsinki principles. All patients involved in the study have provided written informed consent.

RT-qPCR analysis

Briefly, ribonucleic acid (RNA) from the clinical fresh tissues and collected cell samples was extracted using the Trizol reagent, followed by reverse transcription into complimentary deoxyribose nucleic acid (cDNA) utilizing reverse transcriptase from TenGen Biomedical Co. Ltd. (Shanghai, China). The reaction setup was prepared according to the real-time PCR kit instructions from TenGen Biomedical Co. Ltd., utilizing pre-mixed Syber Green, with glyceraldehyde-3-phosphate dehydrogenase (GAPDH) serving as the reference for target amplification. Each group was performed in triplicate to determine the Ct value, facilitating the relative quantification for statistical analysis. The relative expression of the target gene in each experimental group was calculated using the formula $rQ = 2^{-\triangle\triangle CT}$. The selected primers were synthesized by Shanghai Sangong Biotechnology Co., Ltd. (Shanghai, China), with sequences as follows:

PNO1 - Forward (PNO1-F): CTCTGCCAGTGTGTCGTCTT.
Reverse (PNO1-R): TTGCCAACTCCCAAGGGTTT.
GAPDH - Forward (GAPDH-F): GCAAATTCCATGGCACCGT.
Reverse (GAPDH-R): TCGCCCCACTTGATTTTGG.

Western blot (WB) analysis

Initially, the cells were lysed and centrifuged to collect total proteins, which were quantified using a bicinchoninic acid (BCA) protein assay kit. Samples were denatured in a metal bath before loading 30 μg of protein per well for electrophoresis on a 10% sodium dodecyl sulfate-polyacrylamide gel electrophoresis (SDS-PAGE) gel. Further, the separated proteins were then transferred to a polyvinylidene fluoride (PVDF) membrane using the wet transfer method and blocked with 5% skimmed milk for 1 h. The membrane was incubated with primary antibodies diluted in buffer (1:1000) at 4 °C overnight, including PNO1 (21059-1-AP, Proteintech Inc., Wuhan, China), anti-Oct4 (ab109183, Abcam Ltd., Waltham, USA), anti-Sox2 (ab92494, Abcam), anti-p-AKT (ab283852, Abcam), anti-p-GSK-3β (ab32391, Abcam), anti-beta Catenin (ab246504, Abcam), and anti-GAPDH (Cat# ab181602, Abcam). Further, the membranes were washed with the buffer and incubated with goat anti-rabbit secondary antibody (diluted 1:1000) at 37 °C for 1 h. After washing with tris-buffered saline with Tween 20 (TBST), the membrane was developed using an enhanced chemiluminescence (ECL) substrate. The gray values were scanned, and the ratio of the experimental group to the control was normalized using GAPDH as an internal reference.

Cell transfection

Cells in the logarithmic growth phase were adjusted to the appropriate density and seeded for 24 h. After cell confluence reached approximately 70-80%, transfection was carried out using Lipo6000™ transfection reagent (Biyuntian Biotechnology, Shanghai, China, Cat: C0526). The cells were transfected with either short hairpin negative control (sh-NC), sh-PNO1, pcDNA3.1, or pcDNA3.1-PNO1 constructs (Gemma Biotherapeutics Inc.

London, UK). After a 5-hour incubation period for adsorption, the medium was replaced with a fresh, complete medium to continue the culturing process.

CCK-8 assay

The proliferation ability of ovarian cancer cells was determined by incubating for 0 h, 24 h, 48 h, and 72 h using a Cell-Counting kit (CCK)-8 (Cat#CK04, Dojindo Molecular Technologies, Rockville, USA) following the manufacturer's instructions. Briefly, cells were seeded in 96-well plates at a density of 2×10^3 cells per well and incubated overnight for proper cell attachment. Further, the cells in different treatment groups were incubated with CCK-8 working solution (10 µl) in culture medium (150 µl) at 37 °C for 2 h. Finally, the absorbance values at 450 nm were measured using a multimode microplate reader (Thermo Fisher Scientific, Waltham, USA).

EdU staining

Cells at their peak transfection efficiency were seeded into 6-well plates. After 24 h, the BeyoClick™ EdU-647 Cell Proliferation Detection Kit (Beyotime Biotechnology Co. Ltd., Shanghai, China) was utilized according to the manufacturer's instructions. Hoechst 33,342 was applied to counter-stain the nuclei. It should be noted that the cells were incubated at room temperature away from light for 10 min. Subsequently, images were captured using an inverted fluorescence microscope for documentation.

Transwell migration/invasion assay

The Matrigel-based matrix gel (BD Biosciences, Franklin Lakes, USA) was diluted with a serum-free medium. The medium was filled in the upper Transwell chamber (Corning Inc., Corning, USA) and then left in a 37 °C water bath for 4–5 h for solidification of the medium. Cells were digested with trypsin at their peak transfection phase, counted, and resuspended to create a cell suspension. 100–150 µl of the cell suspension (2×10^5 cells/mL) was placed in the upper chamber. In the lower chamber of the Transwell, a 10% FBS complete medium was added, and the setup was incubated at 37 °C in a 5% CO_2 incubator for 24 h. Finally, the cells were then fixed with anhydrous methanol and stained with a 2% crystal violet for 15–30 min. The cells on the surface of the upper chamber membrane were carefully removed and counted using an inverted microscope.

Scratch assay

The fully digested ovarian cancer cells were suspended in a complete medium to halt the digestion process and evenly distributed across the plate. A straight edge or a line drawn on the back of a 6-well plate served as a guide for creating a scratch on the cell layer with a marker pen. Further, cells were rinsed with phosphate-buffered saline (PBS) to remove the detached cells, and a serum-free medium was added. After 24 h, the scratches were imaged, analyzing cell migration using the Image J software.

Sphere formation assay

Ovarian cancer cells were seeded at a density of 1×10^3 cells per well in a serum-free Dulbecco's modified Eagle medium (DMEM)/F12 medium supplemented with B27 (1:50, Invitrogen, Waltham, USA), 20 ng/mL epidermal growth factor (EGF, Sigma-Aldrich), and 20 ng/ml basic fibroblast growth factor (bFGF, Sigma-Aldrich) in ultra-low attachment 6-well plates (Corning Inc.). Further, cells were cultured at 37 °C with 5% CO_2 for a certain period by regularly changing the medium. After 14 days of culture, spheres with a diameter greater than 75 µm were counted using an inverted microscope.

In vivo investigations

For in vivo investigations, healthy female Balb/c-nu nude mice ($n = 12$) were acquired from Changzhou Cavins Animal Experimentation Company and housed in a specific-pathogen-free (SPF)-grade facility. The animal experiments were approved by the Animal Care and Use Committee at the Obstetrics & Gynecology Hospital of Fudan University. Initially, the xenograft model was established following the protocol as stated below. Briefly, cells at their peak post-transfection phase were harvested during the logarithmic growth phase, dissociated into a single-cell suspension using 0.25% Trypsin, and collected the cell pellet. Further, the viability was assessed using trypan blue staining, adjusting the cell concentration to 1×10^6 cells/0.1 ml. Then, the cell suspension was subcutaneously injected into the axillary region of the nude mice. The tumor growth in mice maintained in an SPF-grade facility was monitored and measured every 5 days to plot the tumor growth curve. The tumor volume was calculated using the formula: V = L x (W x W)/2, where V is tumor volume, L is tumor length, and W is tumor width. On day 35, the tumors were excised from the euthanized mice, and their weights were recorded. Further, the fresh tumor tissues were fixed in 4% paraformaldehyde, processed, and embedded in paraffin for subsequent immunohistochemical analysis of PNO1 and Ki-67 expression.

Immunohistochemical analysis

The extracted tissue samples from each group of mice underwent a series of preparatory steps, including dehydration, paraffin embedding, and dewaxing. Further, these samples were rehydrated through a graded alcohol series and antigen retrieval using sodium citrate solution with heat-induced epitope retrieval and natural cooling. Then, the endogenous peroxidase activity was quenched using hydrogen peroxide, blocking the slides at room temperature. Various primary antibodies, including PNO1 (21059-1-AP, Proteintech Inc.) and Ki-67 (Cat#:ab245113, Abcam), were applied and incubated at 37 °C for 1 h. Further, the tissue samples were incubated with the horseradish peroxidase-conjugated secondary antibody and visualized using 3, 3'-diaminobenzidine (DAB kit; Cat. no. DAB-0031; Fuzhou Maixin Biotech Co., Ltd., Fuzhou, China). Then, slides were counterstained with hematoxylin, dehydrated through a graded alcohol series, cleared in xylene, and mounted with a neutral resin adhesive. Finally, the slides were visualized using a microscope.

Statistical analysis

Data presented as the mean ± standard deviation (S.D.) were statistically analyzed using both GraphPad Prism 7 and SPSS 20.0. The survival analysis was conducted using Kaplan-Meier (KM) survival curves. The log-rank test was applied to assess the differences in survival times. The data between multiple groups were compared using a one-way analysis of variance (ANOVA) for multiple groups and a Student's *t*-test for comparisons between two groups. A *P*-value of less than 0.05 was considered statistically significant.

Results

High PNO1 expression in ovarian cancer is linked to poor prognosis

Analyzing The Cancer Genome Atlas Ovarian Cancer (TCGA-OV) database using the GEPIA online tool indicated a notable increase in the expression levels of PNO1 in the ovarian cancer tissues (Fig. 1A). Furthermore, 50 pairs of ovarian cancer and adjacent non-cancerous tissues collected from clinical sources were analyzed, revealing a substantial elevation ($P<0.01$) in PNO1 levels by RT-qPCR analysis in the cancerous tissues over the paracancerous tissues (Fig. 1B). The WB analysis on 10 pairs of ovarian cancer and adjacent non-cancerous tissues confirmed the improved expression of PNO1 protein in the cancerous tissue samples (Fig. 1C). Further, the immunohistochemical analysis corroborated the significantly increased expression of PNO1 in the cancer tissues compared to the adjacent non-cancerous tissues. To investigate the impact of PNO1 expression on the survival outcomes of ovarian cancer patients, the patients were divided into two groups based on the median expression level of PNO1, including a high-expression group ($n=25$) and a low-expression group ($n=25$). The median expression value of PNO1 in ovarian cancer tissues was used as the cutoff value to divide ovarian cancer patients into two groups. The KM survival analysis was employed to determine the overall survival (OS) rates of these patients (Fig. 1D). The findings revealed that the high-expression group of patients showed a significantly poorer prognosis compared to those with the high-expression group of patients (Fig. 1E). The association between PNO1 expression and the clinicopathological characteristics of ovarian cancer was statistically analyzed using the chi-square test (Table 1). It was observed that PNO1 expression was significantly associated with the T stage, chemotherapy cycle, chemoresponse, FIGO stage, tumor differentiation, and lymph node metastasis ($P<0.05$). Nevertheless, it showed no significant relationship with patient age, tumor type, or menopausal status.

PNO1 knockdown inhibited the proliferation, invasion, and sphere-forming characteristics of ovarian cancer cells

Considering the normal ovarian cells, the IOSE80 cell line, as the control treatment group, PNO1 expression was examined in ovarian cancer cell lines (CAOV3, SKOV3, OVCAR-3, and A2780) in vitro (Fig. 2A). The results indicated that PNO1 expression was significantly higher in ovarian cancer cell lines compared to the normal ovarian cells. Specifically, the PNO1 expression was notably higher in OVCAR-3 and SKOV3 than in the other kinds of cancer cells. Therefore, these two cell lines with higher PNO1 expression were selected to investigate further the impact of PNO1 on the ovarian cancer cell phenotype. A short-hairpin RNA (shRNA) targeting PNO1 (sh-PNO1) was employed to reduce PNO1 levels in OVCAR-3 and SKOV3 cells, and the knockdown efficacy was evaluated through WB analysis. It was observed that sh-PNO1#1 and sh-PNO1#2 substantially decreased the expression levels of PNO1 by over 50% in these cell lines (Fig. 2B, $P<0.01$). Further, the effects of PNO1 knockdown on OVCAR-3 and SKOV3 cells revealed the inhibition of proliferation, invasion, and tumor stemness of ovarian cancer cells compared to the control sh-NC (Fig. 2C). The EdU assay results demonstrated a significant reduction in EdU-positive cells following PNO1 knockdown (Fig. 2D). Similarly, the PNO1 knockdown significantly decreased migration and invasion abilities (Fig. 2E), as well as spheroidogenic activity of the ovarian cell lines (Fig. 2F). Further, the cell scratch assay confirmed that PNO1 knockdown reduced the migration ability of ovarian cancer cells (Fig. 2G). The WB analysis showed that the PNO1 knockdown significantly reduced the expression levels of cancer stem cell markers, i.e., OCT4 and SOX2 in OVCAR-3 and SKOV3 cells compared to the control treatment group, sh-NC (Fig. 2H).

PNO1 overexpression promotes the proliferation, invasion, and stemness characteristics of ovarian cancer cells

Prior to exploring the effects of PNO1 overexpression on the characteristics of cancer cells, an overexpression plasmid (pcDNA3.1-PNO1) was constructed, and the A2780 cell line was transfected using exogenous liposomes. Initially, the efficiency of PNO1 expression was detected by the WB analysis, indicating that the PNO1 expression in the pcDNA3.1-PNO1 group was significantly ($P<0.01$) elevated compared with the pcDNA3.1 vector (Fig. 3A). Further, the exogenous overexpression of PNO1 in A2780 cells in the pcDNA3.1-PNO1 group revealed a significant increase in their proliferation (Fig. 3B, C), migration, and invasion abilities (Fig. 3D), as well as a sphere-forming characteristic feature (Fig. 3E) compared with the control pcDNA3.1 group. In addition, the cell scratch assay confirmed that the overexpression of PNO1 could increase the migration ability of ovarian cancer cells (Fig. 3F). The WB analysis demonstrated that the expression levels of the OCT4 and SOX2 proteins were significantly higher in the pcDNA3.1-PNO1 group compared to the control pcDNA3.1 group ($P<0.01$, Fig. 3G).

PNO1 regulates the malignant phenotype of ovarian cancer cells by activating the AKT/β-catenin pathway

To further investigate the role of PNO1 in regulating the malignant phenotype of ovarian cancer cells *via* the AKT/β-catenin pathway, we examined the expression of PNO1 and its impact on key molecules in the AKT/β-catenin signaling pathway. It was observed that the PNO1 knockdown significantly reduced the expression levels of phosphorylated AKT (p-AKT), phosphorylated GSK-3β (p-GSK-3β), and active β-catenin proteins in the selected two types of ovarian cancer cells. In contrast, the expression levels of total AKT, GSK3β, and GAPDH

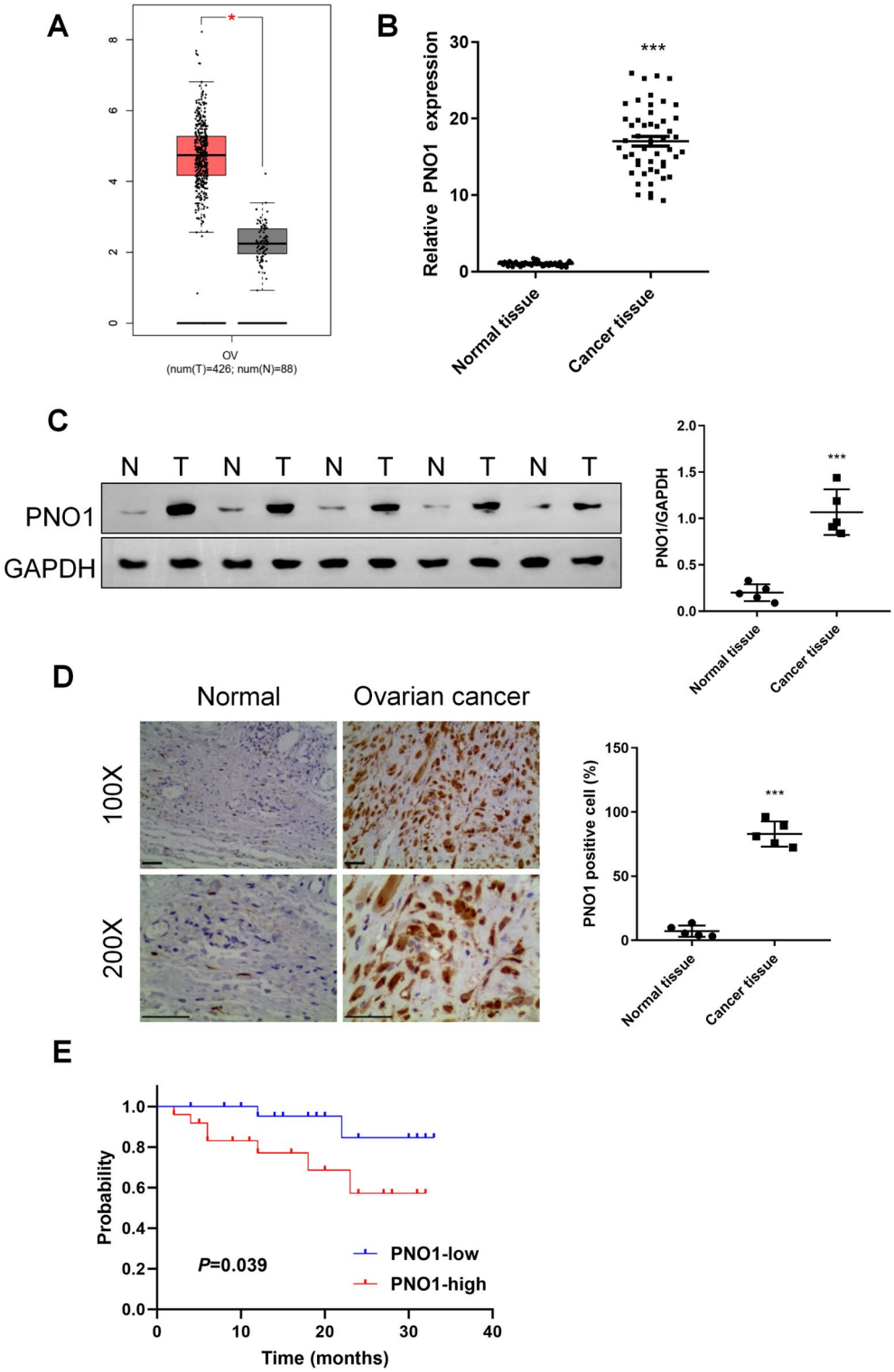

Fig. 1. Analyzing PNO1 Expression and Its Prognostic Significance in Ovarian Cancer. (**A**) The GEPIA online tool on the TCGA-OV database indicates highly expressed PNO1 in ovarian cancer. (**B**) The qRT-PCR analysis assesses PNO1 expression in 50 pairs of ovarian cancer tissues and adjacent non-cancerous tissues ($P < 0.001$). (**C**) Western Blot (WB) analysis presents the expression levels of PNO1 protein in 5 pairs of ovarian cancer tissues and adjacent non-cancerous tissues ($P < 0.001$). (**D**) Immunohistochemical analysis presents PNO1 protein expression in a pair of ovarian cancer tissues and adjacent non-cancerous tissues ($P < 0.001$). Scale bar: 50 μm. (**E**) The KM survival analysis assesses the overall survival (OS) rate of patients with high PNO1 expression.

Diagnostic features	PNO1 high-expression group (n=25)	PNO1 low expression group (n=25)	X^2	P
Age (years)				
≥ 50	17	11	2.922	0.087
< 50	8	14		
Tumor type				
Serous	17	14	1.657	0.799
Clear cell	2	1		
Endometrioid	2	3		
Mucinous	3	5		
Other	1	2		
T stage				
T1	5	10	8.273	0.041
T2	3	8		
T3	8	4		
T4	9	3		
Chemotherapy cycles				
≤ 6	16	22	3.95	0.047
> 6	9	3		
Chemoresponse				
Well	9	18	6.522	0.011
Poor	16	7		
Menopause				
Yes	15	9	2.885	0.089
No	10	16		
Differentiation				
Medium-high differentiation	10	18	5.195	0.023
Low differentiation	15	7		
FIGO stage				
I-II	9	16	3.92	0.048
III-IV	16	9		
Lymph node metastasis				
Yes	13	6	4.16	0.041
No	12	19		

Table 1. The summary presents the correlation between PNO1 and clinicopathologic factors in patients with ovarian cancer.

proteins remained essentially unchanged (Fig. 4A). Further, the results were validated by pretreating the cells with the AKT pathway activator (SC79) and establishing the experimental groups, such as sh-NC, sh-PNO1, SC79, and sh-PNO1 + SC79. The CCK-8 assay results showed that SC79 treatment significantly alleviated the reduction in the proliferation of cells observed after PNO1 knockdown (Fig. 4B). Further, the WB analysis of the expression levels of p-Akt, p-GSK-3β, and active β-catenin proteins within the pathway revealed that the expression levels of intracellular p-AKT, p-GSK-3β, and active β-catenin proteins were significantly increased in the SC79 group. Compared with the SC79 group, the SC79 + sh-PNO1 group showed reduced expression levels of PNO1, p-AKT, p-GSK-3β, and active β-catenin proteins, which were significantly alleviated in the SC79 + sh-PNO1 group (Fig. 4C). Subsequently, several assays for cell proliferation, migration, invasion, and tumor spheroidogenic abilities indicated that PNO1 knockdown reduced these activities compared with the sh-NC group. Contrarily, the SC79 treatment group enhanced the proliferation (Fig. 4D), invasion (Fig. 4E), and tumor sphere formation ability of PNO1-expressed cells compared with the sh-NC group (Fig. 4F). Accordingly, the SC79 treatment could alleviate the decrease in cell proliferation, migration, invasion, and tumor spherogenicity induced by PNO1 knockdown (Fig. 4D–G). In addition, pcDNA3.1 and pcDNA3.1-PNO1 were transfected into A2780 cells to validate further the role of PNO1 in ovarian cancer cell lines. The WB analysis demonstrated that PNO1 overexpression significantly increased the expression levels of phosphorylated AKT (p-AKT), phosphorylated GSK-3β (p-GSK-3β), and active β-catenin proteins in the ovarian cancer cells while maintaining the basic consistency in the expression levels of total AKT, GSK3β, and GAPDH proteins (Fig. 4H). These findings suggested that PNO1 might play a crucial role in the activation of the AKT/β-catenin signaling pathway, which in turn could influence the malignant phenotype of ovarian cancer cells.

Knocking down PNO1 inhibited the proliferation of ovarian cancer cells in vivo

A nude mouse xenograft model of ovarian cancer based on OVCAR-3 cells was established. Further, the long and short diameters of the tumors were measured every 5 days to estimate the tumor growth in terms of tumor

size and plot the tumor growth curve (Fig. 5). It was observed that the volume of subcutaneous tumors in mice with PNO1 knockdown was significantly reduced ($P < 0.01$, Fig. 5A). The PNO1 knockdown mice exhibited a significant reduction in the weights of excised tumors($P < 0.01$, Fig. 5B). Further, the immunohistochemical analysis was used to assess the expression levels of PNO1 and Ki-67 proteins in the subcutaneous tumor tissues of different treatment groups (sh-NC and sh-PNO1). These findings demonstrated that PNO1 knockdown significantly decreased the expression levels of both PNO1 and Ki-67 in the tumor tissues (Fig. 5C, D). In addition, a WB analysis was conducted to measure the expression levels of PNO1, p-AKT, AKT, p-GSK-3β, and active β-catenin in the tumor tissues. The results revealed that PNO1 knockdown significantly reduced the expression levels of p-AKT, p-GSK-3β, and active β-catenin proteins in the transplanted tumor tissues. In contrast, the expression levels of total AKT, GSK3β, and GAPDH proteins remained consistent (Fig. 5E).

Discussion

In this study, we explored the role of PNO1 in ovarian cancer for the first time, revealing that high PNO1 expression could be significantly associated with poor prognosis and reduced survival rates in patients. PNO1 knockdown, both in vitro in cancer cells and in vivo in nude mice, effectively hindered the malignant proliferation, migration, and invasion abilities of ovarian cancer cells. As anticipated, the overexpression of PNO1 resulted in the contrary effects, validating the results. Further, the mechanistic investigations indicated that PNO1 knockdown suppressed the AKT/β-catenin signaling pathway, thereby inhibiting the malignant cell phenotype. Thus, our findings suggested that PNO1 promoted the progression of ovarian cancer by modulating the Wnt signaling pathway. Typically, the cancer cells require enhanced ribosome biogenesis to support increased protein synthesis and sustain unrestricted growth. In recent times, several investigations have demonstrated the correlation between the expression levels of PNO1 and various human cancers, including esophageal, pancreatic, gastrointestinal, and colorectal cancers. Nevertheless, the specific role and mechanism of PNO1 in ovarian cancer remain to be further elucidated. In this study, the TCGA database revealed elevated PNO1 expression in ovarian cancer tissues, corroborated by the clinical specimens and in vitro ovarian cancer cell lines. Moreover, several studies reported that the high PNO1 expression could be associated with poor prognosis in cancer patients. The functional assays showed that PNO1 overexpression significantly enhanced the malignant characteristics of cells. Contrarily, the PNO1 knockdown markedly reduced the tumor cell malignancy, which was validated by various in vivo experiments concerning the tumor-suppressive effect of PNO1 knockdown.

Typically, the Wnt/β-catenin signaling plays a crucial role in various processes critical for embryonic development and tissue homeostasis[18,19]. β-catenin proteins are key components of the Wnt/β-catenin signaling pathway[20,21]. Upon activation, β-catenin stabilizes and moves to the nucleus, associating with the T cell factor/lymphoid enhancer factor (TCF/LEF) family of transcription factors and initiating the transcription of Wnt/β-catenin target genes[20,21]. In general, the highly unstable β-catenin is degraded by the proteasome, which is mediated by the destruction complex[22,23]. The glycogen synthase kinase-3β (GSK-3β) is a central kinase in the destruction complex, responsible for phosphorylating β-catenin, a prerequisite for its proteasomal degradation[24–26]. The activity of GSK-3β often depends on the phosphorylation status of its Ser9 residue[27–33]. The AKT-mediated phosphorylation results in the inactivation of GSK-3β[27–33]. Thus, the AKT/GSK-3β axis plays a crucial role in regulating Wnt/β-catenin signaling activation. In our study, we observed that PNO1 knockdown reduced the expression of p-AKT, p-GSK-3β, and active β-catenin. Further, these inhibition effects were mitigated by the AKT inhibitor SC79. In ovarian cancer cells overexpressing PNO1, a notable increase in the expression of p-AKT, p-GSK-3β, and active β-cateninwas was observed. In addition, SC79 treatment significantly counteracted the suppressive effect of PNO1 knockdown on the malignant cell phenotype. Therefore, PNO1 might promote tumor progression by activating the AKT/Wnt/β-catenin pathway in ovarian cancer. However, the potential mechanism by which PNO1 promotes the phosphorylation of AKT remains unknown, requiring further investigation.

Conclusion

In summary, we explored the expression profile of PNO1 and its role in ovarian cancer. By harnessing data from online repositories, a significant upregulation of PNO1 in ovarian cancer tissues was discovered. These observations were further reinforced by analyzing clinical specimens, establishing a link between elevated PNO1 expression and adverse outcomes in ovarian cancer patients. In addition, the oncogenic role of PNO1 was confirmed through its involvement in the AKT/Wnt/β-catenin signaling pathway in ovarian cancer. Together, our findings shed new light on the oncogenic capabilities of PNO1 in this malignancy.

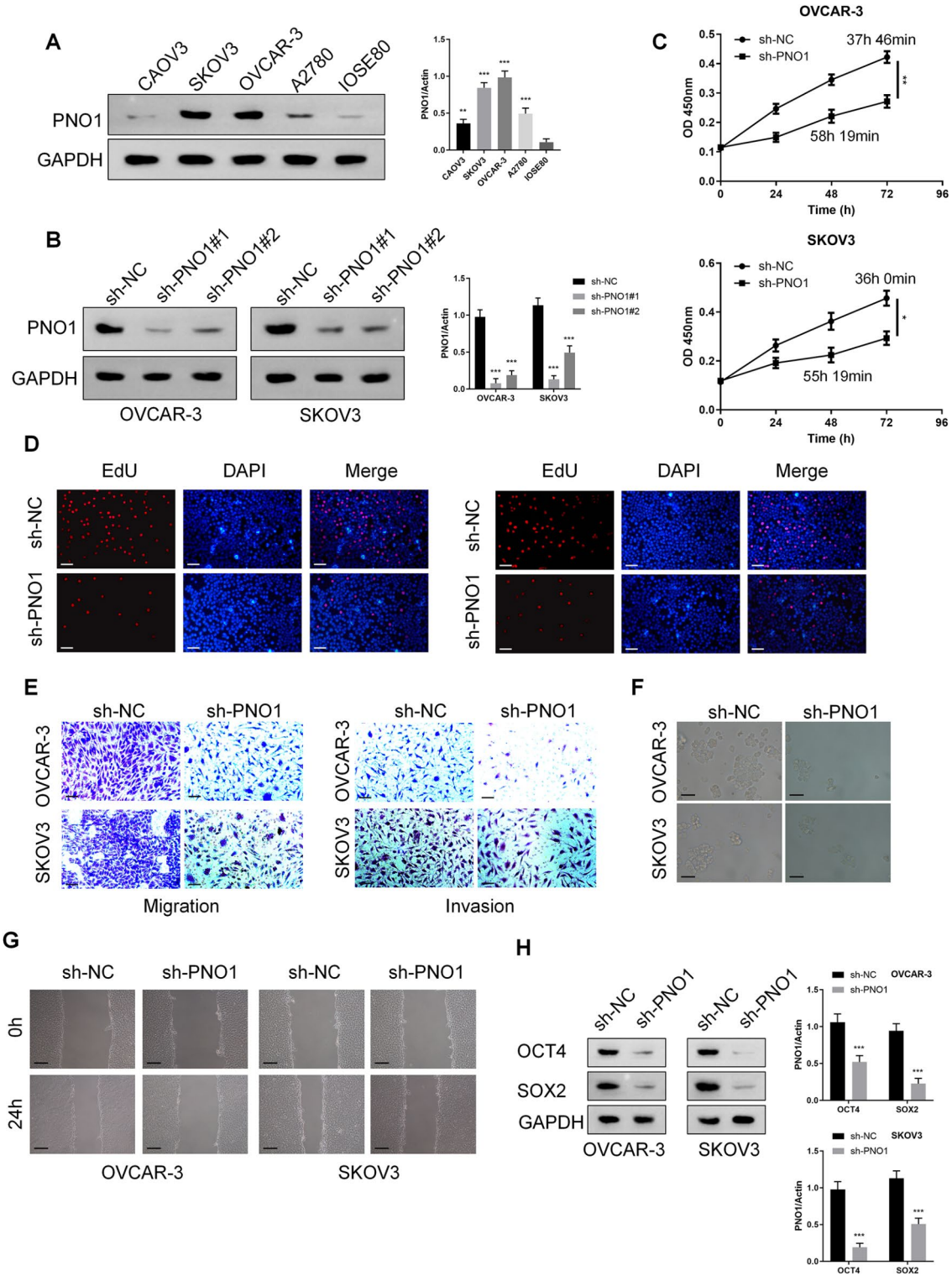
A
CAOV3
SKOV3
OVCAR-3
A2780
IOSE80
PNO1
GAPDH
PNO1/Actin
B
sh-NC
sh-PNO1#1
sh-PNO1#2
OVCAR-3
SKOV3
C
OVCAR-3
sh-NC
sh-PNO1
37h 46min
58h 19min
OD 450nm
Time (h)
SKOV3
36h 0min
55h 19min
D
EdU
DAPI
Merge
E
Migration
Invasion
F
G
0h
24h
H
OCT4
SOX2

◀**Fig. 2**. PNO1 knockdown inhibited the proliferation, invasion, and sphere-forming characteristics of ovarian cancer cells. (**A**) The WB analysis presents expression levels of PNO1 protein in ovarian cancer cell lines (CAOV3, SKOV3, OVCAR-3, and A2780) and the normal ovarian cell line (IOSE80) ($P < 0.05$). (**B**) The WB analysis indicates expression levels of PNO1 protein after sh-PNO1 knockdown (stable knockdown cell line constructed using lentivirus) in OVCAR-3 and SKOV3 cells ($P < 0.01$). (**C**) The CCK-8 assay determines the viabilities of different cell lines (OVCAR-3 and SKOV3 cells) at 0, 24, 48, and 72 h after PNO1 knockdown ($P < 0.01$). The doubling time of cells was marked by each curve. (**D**) The EdU assay indicates the assessment of cell proliferation levels in different groups (sh-NC, sh-PNO1) of OVCAR-3 and SKOV3 cells ($P < 0.01$). Scale bar: 50 μm. (**E**) The Transwell invasion assay presents the invasion ability in different groups (sh-NC, sh-PNO1) of OVCAR-3 and SKOV3 cells. ($P < 0.01$). Scale bar: 50 μm. (**F**) The images present a sphere-forming assay to assess stemness ability in different groups (sh-NC, sh-PNO1) of OVCAR-3 and SKOV3 cells. Scale bar: 50 μm. (**G**) The scratch assay evaluates the migratory ability in different groups of OVCAR-3 and SKOV3 cells (sh-NC, sh-PNO1) ($P < 0.01$). Scale bar: 50 μm. (**H**) The WB analysis presents the protein levels of OCT4 and SOX2 in different groups (sh-NC, sh-PNO1) of OVCAR-3 and SKOV3 cells ($P < 0.01$).

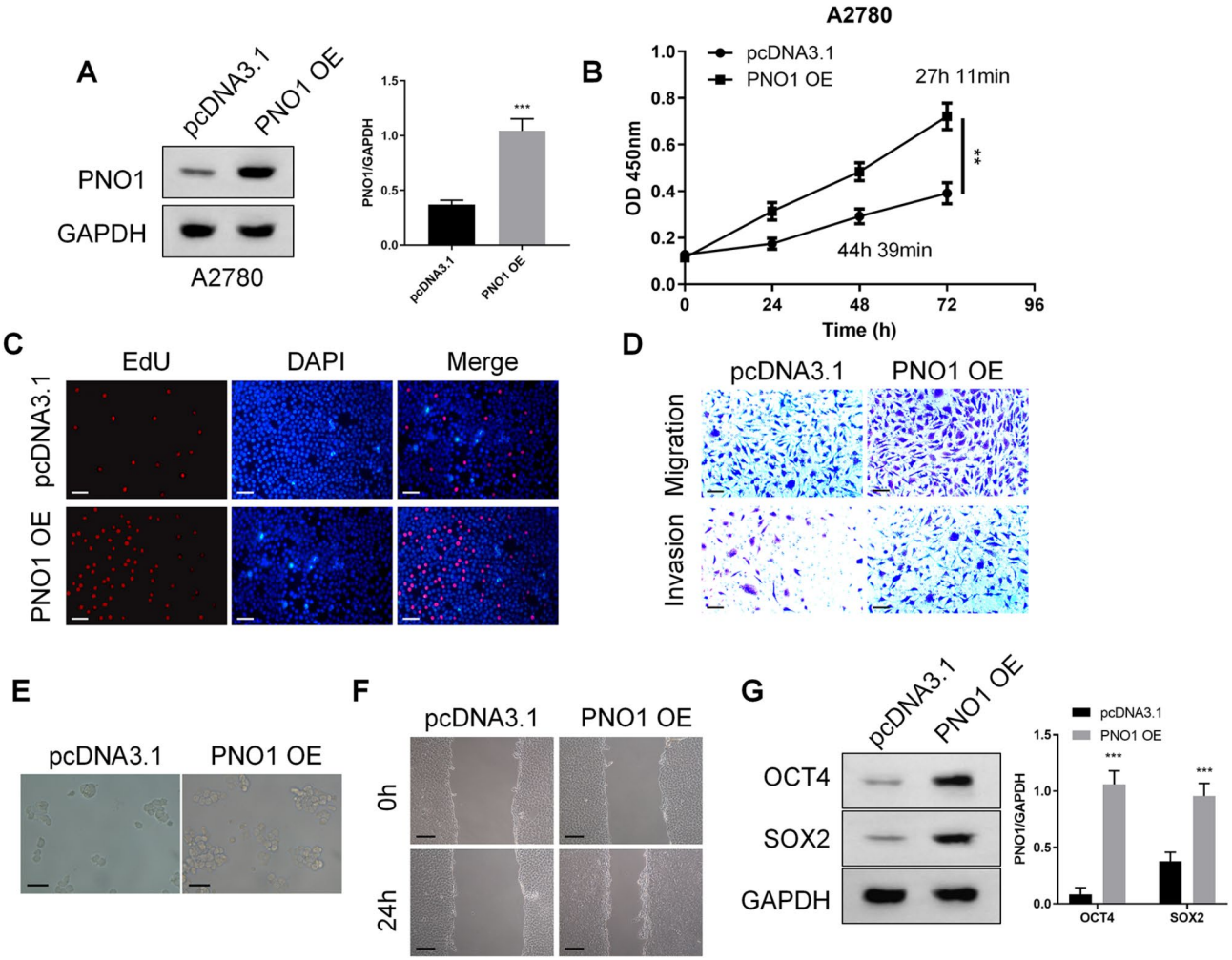

Fig. 3. PNO1 overexpression promotes ovarian cancer cell phenotype. (**A**) The WB analysis validates the overexpression efficiency of PNO1, i.e., pcDNA3.1-PNO1 compared to pcDNA3.1, with a statistically significant difference ($P < 0.01$). (**B**) The CCK-8 assay determines the viability at 0 h, 24 h, 48 h, and 72 h in different groups of A2780 cells (pcDNA3.1, pcDNA3.1-PNO1, $P < 0.01$). The doubling time of cells was marked by each curve. (**C**) The EdU assay presents cell proliferation in different groups of A2780 cells (pcDNA3.1, pcDNA3.1-PNO1) after overexpression of PNO1 ($P < 0.01$). Scale bar: 50 μm. (**D**) The Transwell invasion assay evaluates the invasion ability of A2780 cells in different groups (pcDNA3.1, pcDNA3.1-PNO1) after overexpression of PNO1 ($P < 0.01$). Scale bar: 50 μm. (**E**) The sphere formation assay assesses the stemness capacity in different groups (pcDNA3.1, pcDNA3.1-PNO1) of A2780 cells after overexpression of PNO1 ($P < 0.01$). Scale bar: 50 μm. (**F**) The scratch assay evaluates the migration ability of A2780 cells in different groups (pcDNA3.1, pcDNA3.1-PNO1, $P < 0.01$). Scale bar: 50 μm. (**G**) The WB analysis detects the protein levels of OCT4 and SOX2 in different groups of A2780 cells (pcDNA3.1, pcDNA3.1-PNO1) after overexpression of PNO1 ($P < 0.01$).

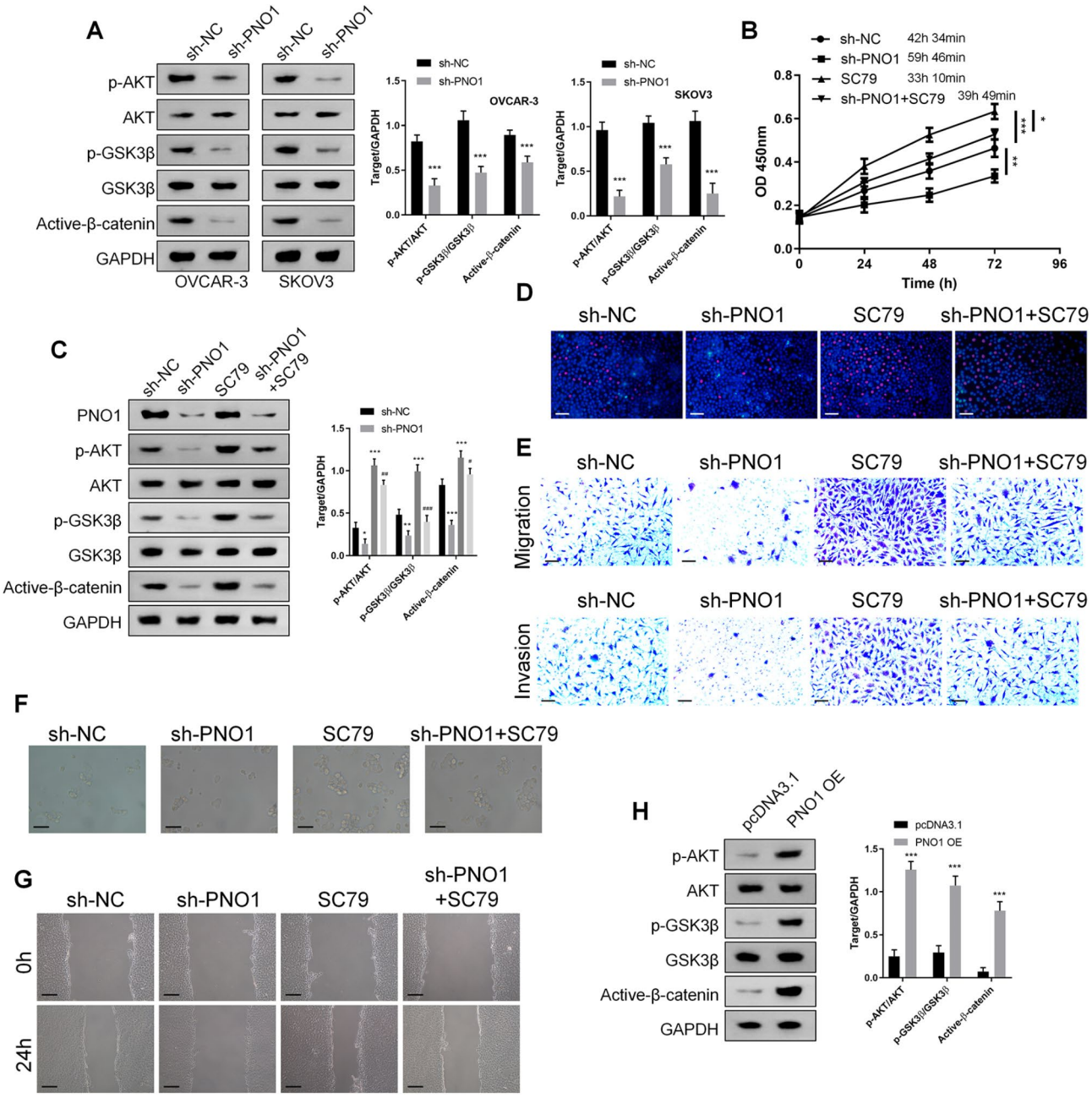

Fig. 4. PNO1 influences the malignant phenotype of ovarian cancer cells through the AKT/β-catenin pathway. (**A**) The WB analysis presents the expression levels of p-AKT, p-GSK-3β, and active β-catenin without affecting total AKT and GSK-3β levels after PNO1 knockdown in OVCAR-3 and SKOV3 cells. (**B**) The CCK-8 assay reveals cell proliferation after PNO1 knockdown and treatment with SC79 ($P < 0.01$). The doubling time of cells was marked by each cell. (**C**) The WB analysis presents the expression levels of PNO1, p-AKT, p-GSK-3β, and active β-catenin proteins in OVCAR-3 cells after PNO1 knockdown and SC79 treatment. (**D**) The EdU assay confirms the proliferation ability after PNO1 knockdown and SC79 treatment. Scale bar: 50 μm. (**E**) The Transwell invasion assay indicates the invasion ability after PNO1 knockdown and SC79 treatment. Scale bar: 50 μm. (**F**) The sphere-forming assay presents the stemness after PNO1 knockdown. Scale bar: 50 μm. (**G**) The scratch assay evaluates the effects of PNO1 knockdown and SC79 on cell migration. (**H**) The WB analysis presents the expression levels of p-AKT, p-GSK-3β, and active β-catenin levels, with no change in total AKT and GSK-3β levels in A2780 cells after PNO1 overexpression.

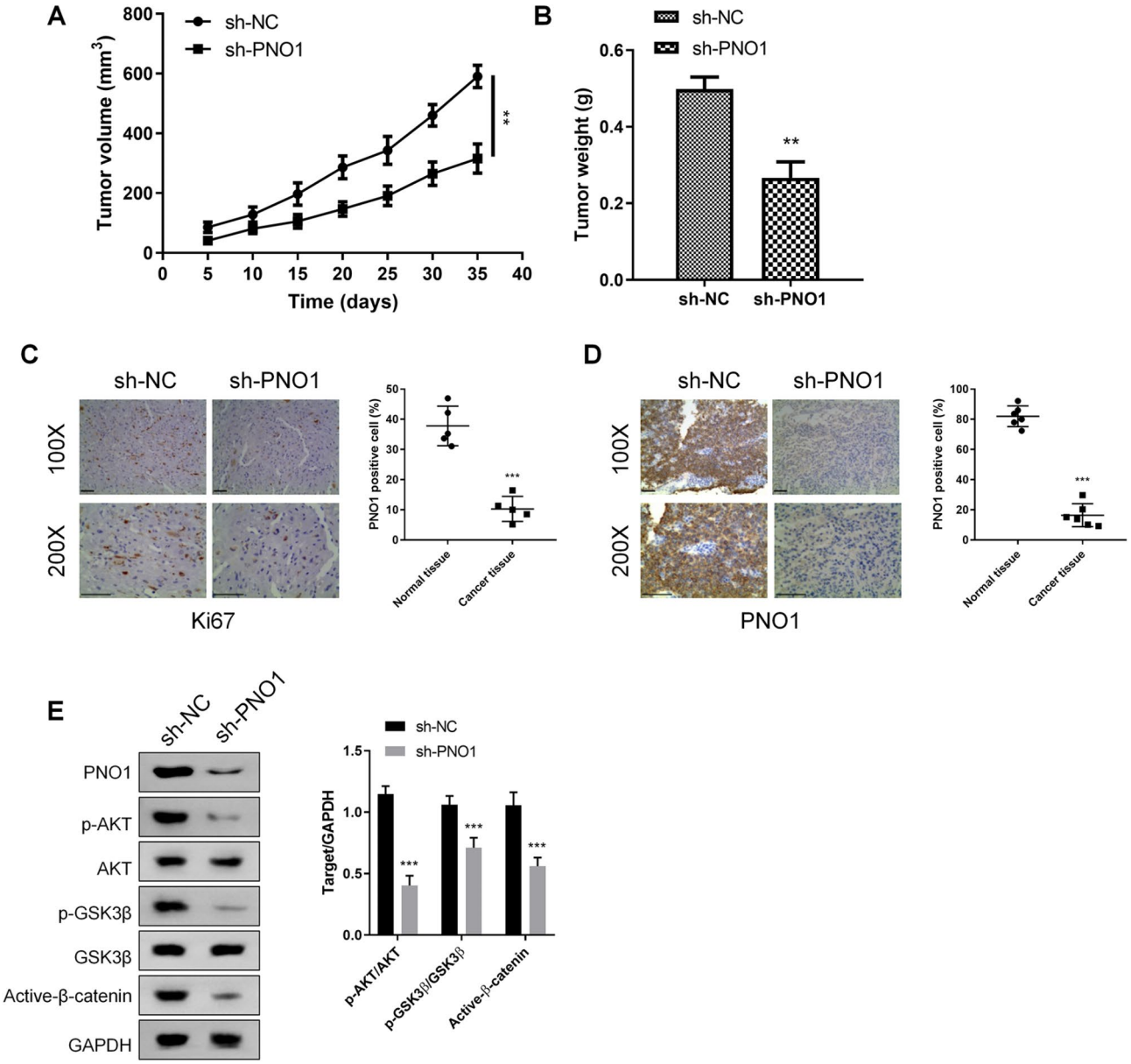

Fig. 5. PNO1 knockdown reduces ovarian cancer cell proliferation in vivo. (**A**) The graph indicates the tumor volume at intervals (5, 10, 15, 20, 25, 30, and 35 days) in the PNO1 knockdown group compared to the control group ($P < 0.01$). (**B**) The graph presents the changes in the tumor weight in the PNO1 knockdown group ($P < 0.01$). (**C**) Immunohistochemical analysis shows the reduced expression level of Ki-67 protein in the PNO1 knockdown group. Scale bar: 50 μm. (**D**) The images show the PNO1 protein expression after the PNO1 knockdown. (**E**) The WB analysis reveals expression levels of PNO1, p-AKT, p-GSK-3β, and active β-catenin proteins in the PNO1 knockdown group, indicating a suppression of the AKT/β-catenin pathway.

Data availability

The datasets used and/or analysed during the current study available from the corresponding author on reasonable request.

Received: 4 July 2024; Accepted: 7 March 2025
Published online: 20 March 2025

References

1. Siegel, R. L., Miller, K. D. & Jemal, A. Cancer statistics, 2020. *CA Cancer J. Clin.* **70** (1), 7–30 (2020).
2. Lino-Silva, L. S. Ovarian carcinoma: pathology review with an emphasis in their molecular characteristics. *Chin. Clin. Oncol.* **9** (4), 45 (2020).
3. Manasa, G., Mascarenhas, R. J., Shetti, N. P., Malode, S. J. & Aminabhavi, T. M. Biomarkers for early diagnosis of ovarian carcinoma. *ACS Biomater. Sci. Eng.* **8** (7), 2726–2746 (2022).

4. Nugawela, D. & Gorringe, K. L. Targeted therapy for mucinous ovarian carcinoma: evidence from clinical trials. *Int. J. Gynecol. Cancer*. **33** (1), 102–108 (2023).
5. Punzon-Jimenez, P., Lago, V., Domingo, S., Simon, C. & Mas, A. Molecular Management of High-Grade Serous Ovarian Carcinoma. *Int. J. Mol. Sci.* **23**(22) (2022).
6. Voutsadakis, I. A. Low-grade serous ovarian carcinoma: an evolution toward targeted therapy. *Int. J. Gynecol. Cancer*. **30** (10), 1619–1626 (2020).
7. Gaona-Luviano, P., Medina-Gaona, L. A. & Magana-Perez, K. Epidemiology of ovarian cancer. *Chin. Clin. Oncol.* **9** (4), 47 (2020).
8. Improta, G. et al. Ovarian clear cell carcinoma: from morphology to molecular biology. *Appl. Immunohistochem. Mol. Morphol.* **27** (9), 631–636 (2019).
9. Han, Z. et al. PNO1 regulates autophagy and apoptosis of hepatocellular carcinoma via the MAPK signaling pathway. *Cell. Death Dis.* **12** (6), 552 (2021).
10. Hu, X. et al. PNO1 inhibits autophagy-mediated ferroptosis by GSH metabolic reprogramming in hepatocellular carcinoma. *Cell. Death Dis.* **13** (11), 1010 (2022).
11. Wang, G. et al. Knockdown of PNO1 inhibits esophageal cancer progression. *Oncol. Rep.*, **45**(5). (2021).
12. Song, M., Bode, A. M., Dong, Z. & Lee, M. H. AKT as a therapeutic target for Cancer. *Cancer Res.* **79** (6), 1019–1031 (2019).
13. Revathidevi, S. & Munirajan, A. K. Akt in cancer: mediator and more. *Semin Cancer Biol.* **59**, 80–91 (2019).
14. Shariati, M. & Meric-Bernstam, F. Targeting AKT for cancer therapy. *Expert Opin. Investig. Drugs*. **28** (11), 977–988 (2019).
15. Peng, Y., Wang, Y., Zhou, C., Mei, W. & Zeng, C. PI3K/Akt/mTOR pathway and its role in Cancer therapeutics: are we making headway?? *Front. Oncol.* **12**, 819128 (2022).
16. Ediriweera, M. K., Tennekoon, K. H. & Samarakoon, S. R. Role of the PI3K/AKT/mTOR signaling pathway in ovarian cancer: biological and therapeutic significance. *Semin Cancer Biol.* **59**, 147–160 (2019).
17. Zhou, J., Jiang, Y. Y., Chen, H., Wu, Y. C. & Zhang, L. Tanshinone I attenuates the malignant biological properties of ovarian cancer by inducing apoptosis and autophagy via the inactivation of PI3K/AKT/mTOR pathway. *Cell. Prolif.* **53** (2), e12739 (2020).
18. Choi, B. Y. Targeting Wnt/beta-Catenin pathway for developing therapies for hair loss. *Int. J. Mol. Sci.*, **21**(14). (2020).
19. Feng, Y. et al. Wnt/beta-Catenin-Promoted macrophage alternative activation contributes to kidney fibrosis. *J. Am. Soc. Nephrol.* **29** (1), 182–193 (2018).
20. He, S. & Tang, S. WNT/beta-catenin signaling in the development of liver cancers. *Biomed. Pharmacother.* **132**, 110851 (2020).
21. Liu, J. et al. Wnt/beta-catenin signalling: function, biological mechanisms, and therapeutic opportunities. *Signal. Transduct. Target. Ther.* **7** (1), 3 (2022).
22. Perugorria, M. J. et al. Wnt-beta-catenin signalling in liver development, health and disease. *Nat. Rev. Gastroenterol. Hepatol.* **16** (2), 121–136 (2019).
23. Russell, J. O. & Monga, S. P. Wnt/beta-Catenin signaling in liver development, homeostasis, and pathobiology. *Annu. Rev. Pathol.* **13**, 351–378 (2018).
24. Schunk, S. J., Floege, J., Fliser, D. & Speer, T. WNT-beta-catenin signalling - a versatile player in kidney injury and repair. *Nat. Rev. Nephrol.* **17** (3), 172–184 (2021).
25. Yu, F. et al. Wnt/beta-catenin signaling in cancers and targeted therapies. *Signal. Transduct. Target. Ther.* **6** (1), 307 (2021).
26. Zhang, X., Dong, N. & Hu, X. Wnt/beta-catenin signaling inhibitors. *Curr. Top. Med. Chem.* **23** (10), 880–896 (2023).
27. Huang, B. et al. Polydatin prevents lipopolysaccharide (LPS)-Induced Parkinson's disease via regulation of the AKT/GSK3beta-Nrf2/NF-kappaB signaling Axis. *Front. Immunol.* **9**, 2527 (2018).
28. Lin, J., Song, T., Li, C. & Mao, W. GSK-3beta in DNA repair, apoptosis, and resistance of chemotherapy, radiotherapy of cancer. *Biochim. Biophys. Acta Mol. Cell. Res.* **1867** (5), 118659 (2020).
29. Pan, J. et al. CD36 mediates palmitate acid-induced metastasis of gastric cancer via AKT/GSK-3beta/beta-catenin pathway. *J. Exp. Clin. Cancer Res.* **38** (1), 52 (2019).
30. Peng, S. et al. AKT/GSK-3beta signaling is altered through downregulation of mTOR during cerebral ischemia/reperfusion injury. *Mol. Biol. Rep.* **49** (5), 3955–3964 (2022).
31. Peng, X. et al. TREM2 inhibits Tau hyperphosphorylation and neuronal apoptosis via the PI3K/Akt/GSK-3beta signaling pathway in vivo and in vitro. *Mol. Neurobiol.* **60** (5), 2470–2485 (2023).
32. Shengyu, C. et al. Selenium alleviates heart remodeling through Sirt1/AKT/GSK-3beta pathway. *Int. Immunopharmacol.* **111**, 109158 (2022).
33. Tang, Z. et al. AKT/GSK-3beta/beta-catenin signaling pathway participates in erythropoietin-promoted glioma proliferation. *J. Neurooncol.* **149** (2), 231–242 (2020).

Author contributions

Conception and design: Min Liu, Lu Qin. Data analysis and interpretation: Lu Qin, Jiao Lu, Qiaohong Qian, Minjie Tang. Manuscript writing: Lu Qin, Minjie Tang, Min Liu. Final approval of manuscript: All authors.

Funding

This work was supported by the project of the Shanghai Municipal Health Commission (No. 2022QN084).

Declarations

Competing interests

The authors declare no competing interests.

Ethics approval and consent to participate

The Ethics Committee of Obstetrics & Gynecology Hospital of Fudan University approved the collection of samples used in this study. The protocol for this study received approval from the Ethics Committee and was conducted in accordance with the Declaration of Helsinki principles. All patients involved in the study provided written informed consent. Each animal experimental procedure gained approval from the Animal Ethics Committee of Obstetrics & Gynecology Hospital of Fudan University. The experimental protocols were validated in accordance with the relevant guidelines and regulations of the Basel Declaration. The study was conducted in accordance with ARRIVE guidelines (https://arriveguidelines.org).

Additional information

Supplementary Information The online version contains supplementary material available at https://doi.org/10.1038/s41598-025-93519-y.

Correspondence and requests for materials should be addressed to M.L.